Title

Laminin N-terminus α31 is upregulated in invasive ductal breast cancer and changes the mode of tumour invasion.

Authors and affiliations:

Lee D. Troughton[1*], Tobias Zech[2], Kevin J. Hamill[1]

[1]Institute of Ageing and Chronic Disease, University of Liverpool, Liverpool, UK.

[2]Institute of Translational Medicine, University of Liverpool, Liverpool, UK.

*Corresponding author

Email leedavid@liverpool.ac.uk

Corresponding address:

Institute of Life Course and Medical Sciences, William Henry Duncan Building, 6 West Derby Street, University of Liverpool, UK, L7 8TX

Abstract

Laminin N-terminus α31 (LaNt α31) is an alternative splice isoform derived from the laminin α3 gene. The LaNt α31 protein is enriched around the terminal duct lobular units in normal breast tissue. In the skin and cornea the protein influences epithelial cell migration and tissue remodelling. However, LaNt α31 has never been investigated in a tumour environment. Here we analysed LaNt α31 in invasive ductal carcinoma and determined its contribution to breast carcinoma invasion. LaNt α31 expression and distribution were analysed by immunohistochemistry in human breast tissue biopsy sections and tissue microarrays covering 232 breast cancer samples. This analysis revealed LaNt α31 to be upregulated in 56 % of invasive ductal carcinoma specimens compared with matched normal tissue, and further increased in nodal metastasis compared with the tumour mass in 45 % of samples. 65.8 % of triple negative cases displayed medium to high LaNt α31 expression. To study LaNt α31 function, an adenoviral system was used to induce expression in MCF-7 and MDA-MB-231 cells. Metabolic activity, 2D cell migration, and invasion into collagen hydrogels were not significantly different between LaNt α31 overexpressing cells and control treated cells. However, LaNt α31 overexpressing MDA-MB-231 cells displayed a striking change in their mode of invasion into laminin-containing Matrigel; changing from multicellular streaming to individual cellular-invasion. In agreement with these results, 66.7% of the tumours with the highest LaNt α31 expression were non-cohesive. Together these findings indicate that breast cancer-associated changes in LaNt α31 expression could directly contribute to tumour invasiveness, and that this little-studied protein may become a therapeutic target.

Abbreviations

Antigen ki-67 (Ki67)

Basement membrane (BM)

Estrogen receptor (ER)

Extracellular matrix (ECM)

Epidermal growth factor (EGF)

Epidermal growth factor receptor (EGFR)

Enhanced green fluorescent protein (eGFP)

Human epidermal growth factor receptor 2 (Her2)

Laminin N terminal protein α31 (LaNt α31)

Laminin-type epidermal growth factor-like (LE-repeat)

Laminin (LM)

Laminin N-terminal (LN domain)

Tumour protein p53 (p53)

Paraffin-fixed formalin-embedded (FFPE)

Progesterone receptor (PR)

Terminal duct lobular unit (TDLU)

Triple negative breast cancer (TNBC)

Introduction

An essential stage of tumour progression is acquisition of an ability to breakthrough an organised extracellular matrix (ECM) structure termed the basement membrane (BM)[1]. Determining the expression and distribution of BM proteins has yielded valuable biomarkers to predict breast cancer outcomes [2-6]. Much of this work has focused on the laminin (LM) family of BM proteins, which are not only essential barrier components, but also act as substrates for tumour cell migration, regulate actin dynamics, influence survival and growth signalling pathways, and maintain quiescence in cancer stem cell niches; all of which functions influence breast cancer progression [7-10]. Here we investigated a relatively unstudied LM-related protein, laminin N-terminus α31 (LaNt α31) that we predicted would

change in cancer and which could therefore represent a new target for therapeutic development [11, 12].

LMs are obligate heterotrimeric proteins comprised of an α, β and γ chain, with each chain derived from one of five α genes (LAMA1-5), one of three β (LAMB1-3), and one of three γ (LAMC1-3), as reviewed in [7, 8, 13]. Through the use of distinct promoters, LAMA3 generates two structurally distinct LMs; a so-called "full-length" variant LMα3b, and the much shorter LMα3a [8, 13-15]. The LaNt proteins are also derived from LM-encoding genes, through intron-retention and polyadenylation within the retained intron [11]. Four LaNt family members have been identified at the transcript level; however, only LaNt α31, derived from the LAMA3 gene, has been confirmed at the protein level [11]. LaNt α31 displays widespread tissue distribution [11] and is enriched in structured regions of ECM surrounding terminal duct lobular units (TDLUs) in normal breast tissue [16].

LaNt α31 functions have only been studied in corneal and skin epithelium to date, where upregulation of LaNt α31 was observed in response to corneal burn wounds or stem cells activation in ex vivo models, and where knockdown in expression reduced the rate at which epidermal keratinocytes close scratch wounds [11, 12]. Mechanistic studies have also indicated a role for this protein in modifying cell adhesion and migration via changes to matrix organisation and adhesion complex maturation [12, 17]. Further indications to LaNt α31 function come from its structure. Although LaNt α31 is smaller than LMs and lacks the coiled-coil domain required for LM trimer formation, it does share structural domains with LMα3b. Specifically, LaNt α31 is comprised a LM N-terminal domain (LN domain) and two LM-type epidermal growth factor-like repeats (LE domains) [11]. LN domains are involved in LM-to-LM interaction, and therefore are essential for laminin network assembly in BMs [7, 18, 19]. LaNt α31 also contains 54 unique amino acids with no homology to known structural motifs but which have allowed specific antibodies to be raised against this protein [11, 12]. Intriguingly the LaNt α31 protein architecture is structurally similar to other members of the laminin superfamily family, the netrins. Netrins are predominantly known as signalling

proteins; however, netrin-4, via its LN domain, can disrupt LM-LM interactions and change the structural characteristics of LM networks [20-22].

While functional data suggest that LaNt α31 could be capable of influencing tumour progression, further rationale for investigating this protein in tumour microenvironment comes from studies of the other, more comprehensively studied, products of the LAMA3 gene. Reduction of LMα3a and LMα3b in breast carcinoma has been independently reported by several groups [23-25], with LMα3b downregulation in tumour vasculature associated with later stage tumours [26]. However, the situation is more complicated than a simple linear relationship, as increased LMα3 has been associated with triple negative breast carcinoma, and increased immunoreactivity that correlated with tumour stage has also been reported with antibodies against conformational epitopes in LMα3β3γ2 (LM332), LMβ3 and LMγ2, the preferred trimerization partners of LMα3a and LMα3b [25, 27].

Here we performed the first investigation into LaNt α31 in breast cancer. Breast tissue from normal and invasive ductal carcinomas were processed for immunohistochemistry with antibodies against LaNt α31, and correlation between staining intensity and pathology determined. LaNt α31 expression was upregulated in cultured breast carcinoma cells in culture and the impact on cellular behaviour was determined. The results revealed that LaNt α31 is increased in tumour tissue and that increased expression changes the mode of invasion of carcinoma cells into LM-rich matrices.

Methods

Ethical approval

The Liverpool Bio-Innovation Hub Biobank conferred ethical approval in writing for the use of samples in this project (REC reference 14/NW/1212, NRES Committee North West – Haydock). Project specific ethical approval for working with human tissue was conferred in writing by the University of Liverpool Research Ethics Committees (approval number:7488).

Antibodies

Mouse monoclonal antibodies raised against human LaNt α31 were described previously [12, 16] and were used at 0.225 µg mL^{-1} for IHC and 1.8 µg mL^{-1} for immunoblotting. Mouse monoclonal antibodies against human LMα3 (clone CL3112) and mouse IgG (both Sigma-Aldrich, St. Louis, Missouri, USA) were used at 0.5 µg mL^{-1}.

Immunohistochemistry

Pilot tissues were obtained from the Liverpool Bio-Innovation Hub Biobank, all other TMA sections were purchased from Reveal Bioscience (product codes: BC02, BC03, BC05, BC06, and BC10; Reveal Bioscience, San Diego, USA) or US Biomax (product code: HBreD145Su02; US Biomax, Rockville, Maryland, USA). Sections were dewaxed and processed using a Leica Bond autostainer with Bond™ Polymer Refine Detection system (Leica Biosystems, Wetzlar, Germany). Briefly, following dewaxing, antigen retrieval was performed by incubating with a Tris/EDTA (pH 9 solution) solution for 20 mins at 60 °C, then endogenous peroxidases were blocked for 5 mins at room temperature with Bond hydrogen peroxide solution. Sections were incubated with primary or isotype-matched control antibodies at room temperature for 30 mins in Bond primary Ab solution (Tris-buffered saline, TBS, containing surfactant and protein stabilizer), then secondary anti-mouse IgG antibodies (<10 µg mL^{-1}) with 10 % v/v animal serum in TBS were added for 15 mins at room temperature. DAB (66 mM) chromogen substrate was added for 20 mins at room

temperature, and counterstaining performed with 0.1 % w/v haematoxylin for 5 mins. At each stage, washing was performed with Bond wash solution (TBS containing surfactant). Sections were finally dehydrated through a series of ascending ethanol concentration and then mounted with Pertex (all reagents Leica Biosystems). Stained tissue sections were imaged on the Aperio ImageScope slide scanner and processed using ImageScope software (Leica Biosystems).

Immunohistochemistry interpretation

TMA cores were graded from 0-3 based on LaNt α31 immunoreactivity. Scores of 0 and 1 were then combined, and expression defined as low, medium, or high. All cores were scored by three independent scorers, and the mean score from duplicate cores used in final analyses. All patient data, including tumour/ node/ metastasis (TNM) status, tumour grade, and IHC marker scores (antigen ki-67 [ki67], epidermal growth factor receptor [EGFR], human epidermal growth factor receptor 2 [Her2], oestrogen receptor [ER], and progesterone receptor [PR]) were provided by Reveal Biosciences. Data were rounded to the nearest integer for intensity scores where required. For Ki67 percentage cell staining, scores were grouped as 0, 6, 6-10, or >10%, as provided by Reveal Biosciences.

Cell culture

MCF-7 [28] and MDA-MB-231 [29] cells were cultured in high glucose (4.5 g L^{-1}) Dulbecco's Modified Eagle Medium (DMEM) (Sigma-Aldrich) supplemented with 10 % Foetal Calf Serum (FCS, LabTech International Ltd, Heathfield, East Sussex, UK) and 4 mM L-glutamine (Sigma-Aldrich).

LaNt α31 expression

Full length *LAMA3LN1-eGFP* and *eGFP* adenoviral particles were prepared and used as previously described [12]. Transduction efficiency was determined by live fluorescent imaging at the time of analysis and expression confirmed by immunoblotting after 24 hours. Cells were homogenized by scraping into urea/ sodium dodecyl sulphate (SDS) buffer (10 mM Tris-HCl pH 6.8, 6.7 M Urea, 1 % w/v SDS, 10 % v/v Glycerol and 7.4 μM

bromophenol blue, containing 50 μM phenylmethysulfonyl fluoride and 50 μM N-methylmaleimide, all Sigma-Aldrich). Lysates were sonicated and 10 % v/v β-mercaptoethanol added (Sigma-Aldrich). Proteins were separated by SDS-polyacrylamide gel electrophoresis (SDS-PAGE) using 10 % polyacrylamide gels (1.5 M Tris, 0.4 % w/v SDS, 10 % acrylamide/ bis-acrylamide; electrophoresis buffer; 25 mM Tris, 190 mM glycine, 0.1 % w/v SDS, pH 8.5 all Sigma-Aldrich). Proteins were transferred to nitrocellulose membranes (Biorad, California, USA) using the Biorad TurboBlot™ system and blocked for one hour at room temperature in Odyssey® TBS-Blocking Buffer (Li-Cor BioSciences, Lincoln, Nebraska, USA). The blocked membranes were incubated overnight at 4°C with primary antibodies diluted in blocking buffer, then probed for 1 hour at room temperature with IRDye® conjugated secondary antibodies against mouse IgG (800CW) raised in goat (LiCor BioSciences) diluted in Odyssey® TBS-Blocking Buffer buffer at 0.05 μg mL^{-1}. Membranes were imaged using the Odyssey® CLX 9120 infrared imaging system and Image Studio Light v.5.2 (LiCor BioSciences) used to process scanned membranes.

Resazurin reduction assay

Transduced or non-transduced cells were plated in triplicate at 1.5 x 10^4 cells/well of a 96-well plate (Greiner-Bio One, Kremsmunster, Austria). After 24 hours culture media was replaced with serum-free and phenol red-free media containing 44 μM resazurin sodium salt (Sigma-Aldrich) [30]. The cells were then incubated for 2 hours. The media was removed and transferred to a black 96-well plate (Greiner-Bio One) and fluorescence measured at 570 nm using a SPECTROstar plate reader (BMG LABTECH, Ortenberg, Germany).

2D migration assays

For gap closure assays, cells were seeded into ibidi® 2-well culture inserts (ibidi, Martinsried, Germany); at 7.0 x 10^4 cells/well (MCF-7) or 8.0 x 10^4 cells/well (MDA-MB-231). Culture inserts were carefully removed after 6 hours, cell debris washed away, and the gap margin imaged using brightfield optics on a Nikon TiE epifluorescence microscope with a

10X objective at 0 and 16 hours (Nikon, Tokyo, Japan). Gap closure was measured as a percentage relative to starting area using the freehand tool in image J (NIH, Bethesda, MA).

For low-density migration assays, cells were seeded at 5.0 x 10^4 cells/well of a 12-well plate, then imaged every 2 minutes over a 2-hour period using a 20X objective on a Nikon Eclipse Ti-E fluorescent microscope adapted for live cell imaging. Individual cells were tracked using the MTrackJ plugin on image J and migration speed calculated.

Inverted invasion assay

Inverted invasion assays were performed as previously described [31-33]. Briefly, 100 µL of 1 mg mL^{-1} rat tail collagen I (Corning Inc., New York, USA) or 4 mg mL^{-1} Matrigel® from Engelbreth-Holm-Swarm (EHS) mouse sarcoma [34], was pipetted on top of Transwell® 24-well, 0.8 µm, polycarbonate inserts (Corning). Then collagen was gelled through addition of 9.2 mM NaOH. Once gelled, the inserts were inverted and 100 µL of cell suspension containing 8.0 x 10^5 cells were added to the lower surface. The transwells were than incubated for 4 hours to allow the cells to attach before returning to the original position with basal side downward. 1 mL of serum-free media was pipetted into the lower chamber of the transwell, and 100 µL of normal culture media supplemented with 25 ng mL^{-1} EGF, as a chemoattractant, was added to the upper chamber [35]. After 72 hours, the cells were fixed with 3.7 % v/v formaldehyde for 30 mins, permeabilised with 0.05 % v/v Triton X-100 then stained for 1 hour with DAPI (Sigma-Aldrich). The inserts were mounted onto a glass coverslip and imaged with a Zeiss Marianas (3i) spinning-disk confocal microscope by taking a z-stack with images every 5 µm, using SlideBook 5.5 software (3i, Intelligent Imaging Innovations Ltd, London, UK).

An algorithm was generated to automatically measure the DAPI stained nuclei in each slice of the z-stack. The average nuclei size was established by taking a range of manual measurements through the different planes of the z-stack. The average was used to set: i) the intensity threshold for distinguishing nuclei fluorescence from background as *t=1000*, ii) the expected nuclei size *s=240* pixels, corresponding to an area of 101.4 µm or a

radius of 5.68 µm, ii) the lower size threshold *s^-=120* pixels (area = 50.7 µm or a= radius of 4.02 µm), below which captured objects were not considered to be nuclei and iv) the upper size threshold *s^+ = 400* pixels (area 169 µm or radius of 7.33 µm), above which the captured object was assumed to be an artefact. For each image slice, the image was imported and a coarse segmentation of the nuclei performed by thresholding at the intensity value *t* to achieve a binary nuclei/non-nuclei image. Any nuclei within an absolute distance of 0.65 µm or 1 pixel were connected to take into account noise, and an initial index taken of the distinct identified nuclei candidates, while measuring the size of each nuclei.

Individual cells were then identified as follows: i) any identified object under *s^-*, *s/2* pixels or over *s^+* pixels in size was considered to be noise, ii) any captured object within the thresholds *s/2* and *3s/2* was considered to be one nuclei, iii) any remaining captured object which was larger than *3s/2* in size was considered to be a cluster of nuclei which could not be split due to the resolution of the image. In these cases, the number of cells in the cluster was calculated as *(cluster size) / s*, rounded to the nearest integer. The following measures were then taken: i) total luminance of the cell image, ii) PixCount: the number of pixels considered to be a cell after thresholding, corresponding to the total area in microns of the region considered to contain a cell. iii) Cell Count: the total number of cells identified, including those estimated from cell clusters, iv) Entropy: a measure of randomness of the thresholding data, which identified how clustered the cells in the image were.

Data analyses

Microsoft Excel (Microsoft, Washington. USA), Graphpad Prism v.6 (Graphpad Software, California, USA), or SPSS statistic 24 (IBM Corporation, New York, USA) were used to analyse numerical data and generate graphs. Figures were generated using CoralDraw 2017.The Wilcoxon signed-rank test or Somers' D was used for ordinal data, or Mantel-Cox log-rank test for survival data in immunohistochemistry analyses, and one-way ANOVA with Bonferroni post hoc test were used for continuous variables. Differences were deemed statistically significant where type I error rates were below 5 %.

Results

LaNt α31 and LMα3 display distinct distribution patterns in invasive ductal carcinomas

First we compared the distribution of LaNt α31 and LMα3 in a pilot panel of four normal (Figure 1A), four invasive ductal (Figure 1B) and four triple negative (Er-PR-Her2-) invasive ductal tissue sections (Figure 1C). The LMα3 antibodies used recognise both the LMα3a and LMα3b forms. LaNt α31 and LMα3 displayed very similar distribution in the normal tissue (Figure 1A), primarily restricted to TDLU as previously reported [16]. However, much stronger and more widespread LaNt α31 expression was detected in three of the four invasive ductal and three of four ER-, PR-, Her2- specimens. In the invasive ductal tissue, LaNt α31 displayed a more widespread distribution than LMα3 (arrowheads, Figure 1B), whereas in ER-PR-Her2- cases the LMα3 and LaNt α31 distribution were very similar (Figure 1C). LMα3 has been extensively investigated in breast cancer [23-25]; however, these new data for LaNt α31 indicated potential additional value of investigating this isoform independently from LMα3 in invasive ductal carcinoma.

Figure 1: LaNt α31 is upregulated in ductal carcinoma. Serial sections from formalin-fixed paraffin-embedded human breast tissue processed for immunohistochemistry with mouse monoclonal antibodies against laminin α3, LaNt α31, or mouse IgG- isotype control, (A) uninvolved breast tissue, (B) invasive ductal carcinoma, and (C) ER-, PR-, Her- invasive ductal carcinoma. Scale bars: 500 μm.

LaNt α31 expression is elevated in invasive ductal carcinoma and in nodal metastases compared to primary tumour tissue

To formally determine whether LaNt α31 expression levels change in invasive ductal carcinoma, the relative intensity of cellular immunoreactivity in epithelial-like tissue was compared between normal breast tissue compared with tumour biopsies from the same person, with intensity scored by three independent, blinded scorers (representative examples, Figure 2A, all cores Figure S1A, patient demographics Table 1). These paired analyses revealed LaNt α31 expression to be increased in the cancer specimen in 14 of 25 tumours (56%) , eight had no change, while three displayed decreased expression in the cancer tissue (Wilcoxon signed ranks test, z=-2.67, p=0.008, Figure 2A).

Comparison of staining intensity between cores taken from the primary tumour against those from nodal metastasis from the same person using the same scoring approach, revealed that 13 of the 29 (45%) of the nodal metastasis displayed stronger LaNt α31 staining compared with primary tumour tissue, 12 were scored the same, and four were decreased in the nodal tissue (Figure 2B, Figure S1B, patient demographics Table 1, z=-2.18, p=0.029).

Figure 2: LaNt α31 is upregulated in ductal carcinoma and in lymph node metastases. Formalin-fixed paraffin-embedded human breast tissue microarray sections processed for immunohistochemistry with mouse monoclonal antibodies against LaNt α31. Two separate arrays were used; (A) uninvolved with paired invasive/ in situ ductal carcinoma tissues (N=25), (B) invasive ductal carcinoma with paired node metastases (N=29). Cores were scored as either decreased, no change, or increased staining intensity relative to the paired uninvolved (A) or primary tumour (B) core from the same donor (representative images shown). Stacked columns of percentage of cases in each category were plotted and Wilcoxon signed ranks test used to describe observed relationship. Scale bars: 500 μm.

295 **Table 1-** Patient ages for each study cohort

Study cohort	Mean	Median	Range	N
Invasive ductal carcinoma vs uninvolved	46	45	29-70	25
Invasive ductal carcinoma vs lymph node metastases	47	46	30-69	29
Ductal carcinoma	46	44	21-86	166
Invasive ductal carcinoma	60	57	33-88	132

296

297 ## LaNt α31 upregulation is associated with less proliferative tumours

298 To determine if LaNt α31 immunoreactivity held prognostic value for invasive ductal
299 carcinoma, we processed 166 patients (Table 1) with two cores scored per patient by three
300 independent scorers with the scores defined as “low”, “medium” or “high” LaNt α31 intensity
301 (Figure 3A). First, we asked if LaNt α31 staining intensity was predictive for tumour grade,
302 Ki67 expression (i.e. high proliferation [36, 37]), nodal involvement, or survival (Figure 3B-E,
303 respectively). For tumour grade, although an increased proportion of cores displayed strong
304 LaNt α31 staining in higher grade tumours, this association did not reach statistical
305 significance (d=0.109, p=0.146, Figure 3B). Surprisingly, a negative correlation was
306 observed between Ki67 expression level and LaNt α31 staining intensity (d=-0.3, p=0.006,
307 Figure 3C). The relative proportions of high, medium and low LaNt α31 expression were
308 broadly similar between those cases which presented with nodal involvement and those
309 without (Somers’ d=0.059, p=0.505, Figure 3D).

310 Survival was assessed for the 132 cases where these data were available. To
311 account for the smaller sample size here, LaNt α31 staining intensity was simplified to either
312 low or high expression by combining the medium with the high expression cases. These
313 data revealed that tumours with higher LaNt α31 staining intensity had marginally improved
314 overall survival, although this did not reach statistical significance at an α of 0.05 (low=66%
315 survival, high=76% survival, hazard ratio 1.52, confidence interval 0.8-2.8, p=0.22, Figure
316 3E).

317

Figure 3: LaNt α31 upregulation in ductal carcinoma does not correlate with nodal involvement or tumour grade. Formalin-fixed paraffin embedded human breast tissue microarray sections processed for immunohistochemistry with mouse monoclonal antibodies against LaNt α31. Cores were scored based on LaNt α31 staining intensity from 0-3. Scores of 0 or 1 were combined and designated as low LaNt α31 expression, score 2 as medium expression, and 3 as high expression. (A) Representative example of core scoring. (B-D) Stacked column graphs of percentage of cases with each staining intensity segregated by tumour grade I, II, or III (B), Ki67 expression (C), or by nodal involvement (D). Somers' D was used to describe observed relationships between LaNt α31 staining intensity and the independent variables. (E) Kaplan–Meier survival curve, were LaNt α31 staining intensity was simplified to low or high by pooling medium and high cores. Logrank was used to determine hazard ratio and chi square for significance. Scale bar in (A): 300 μm.

Next, we asked if LaNt α31 staining displayed a relationship with any of the commonly used breast cancer biomarkers (Figure 4). These data revealed a positive association between LaNt α31 and EGFR (EGFR d=0.26, p=0.003, Figure 4A), while observed associations with Her2, ER and PR were each below statistical significance at an α of 0.05 (Figure 4B-D). However, the data suggest a potential weak, negative association with ER (d=-0.12, p=0.056).

The cores from triple negative cancers were analysed separately (Figure 4E, n=38 cores). These data revealed that more than 65 % of the ER- PR- Her2- cores had either medium or high LaNt α31 staining intensity.

Figure 4: Positive correlation between LaNt α31 staining intensity and EGFR expression. Formalin-fixed paraffin embedded human breast tissue microarray sections processed for immunohistochemistry with mouse monoclonal antibodies against LaNt α31. Cores were scored based on LaNt α31 staining intensity from 0-3. Scores of 0 or 1 were

combined and designated as low LaNt α31 expression, scores 2 as medium expression, and 3 as high expression. Stacked column graph of percentage of cases that fall into group after segregation based on pathologist provided grading of immunohistochemistry markers; (A) EGFR, (B) Her2, (C) ER, (D) PR, or (E) ER- PR- Her2- cases. Somers' D was used to describe observed relationship between LaNt α31 staining intensity and independent variable.

LaNt α31 expression does not induce increased 2D migration or invasion in a non-motile cell line

Together the immunohistochemistry findings indicate an association between LaNt α31 staining and a subset of tumours; however, this does not necessarily indicate that expression change contributes to the disease. To address this question, we used an adenoviral system to drive overexpression of LaNt α31 tagged with eGFP (+LaNt α31-eGFP) in two widely used cell lines derived from invasive ductal carcinomas; MCF-7 and MDA-MB-231 (Figure S2A-B). Cells transduced with eGFP only were used to control for adenoviral transduction and eGFP expression. Expression of eGFP or LaNt α31-eGFP had no effect on metabolic activity of either MCF-7 or MDA-MB-231 cells (Figure S2C-D).

MCF-7 cells migrate slowly and do not invade in 3D invasion assays [38-40]. This line was therefore used to assess if induction of LaNt α31 expression was sufficient to increase these behaviours. In gap closure assays (Figure S3A-B), MCF-7 cells expressing LaNt α31 closed the gap more slowly than controls in three out of seven independent experiments; however, overall the differences were not statistically significant (Figure S3B median: MCF-7 83.3 %, +eGFP 79.7 %, +LaNt α31-eGFP 67.8 %, p=0.37). In single cell assays (Figure S3C-D), a small increase in migration speed was observed three out of four independent experiments, although differences between LaNt α31 and control treatments were not statistically significant (mean migration speed +/- S.D. MCF-7 0.31 μm min^{-1} +/-

371 0.13, +eGFP 0.36 µm min^{-1} +/- 0.09, +LaNt α31-eGFP 0.35 µm min^{-1} +/- 0.06, *p*=0.53,
372 determined by ANOVA. Figure S3D).

373 Next, we asked if increasing LaNt α31 expression could induce invasive capabilities
374 in MCF7 using an inverted invasion assay [33, 41], where cells were seeded on the base of
375 a porous membrane then stimulated to invade into a provided matrix and using an EGF
376 gradient as a chemoattractant (Figure S3E-H). As LaNt α31 effects could be LM specific,
377 invasion into two different matrices were analysed; collagen I to mimic the interstitial matrix
378 (Figure S3E-F) and Matrigel, a BM analogue that contains approximately 60 % LM111, 30 %
379 Type IV collagen, and 8 % entactin [34, 42] (Figure S3G-H). As expected, untreated MCF-7
380 cells had very low invasive capabilities into both matrices, and overexpression of LaNt α31
381 did not lead to any significant change in invasion depth (mean +/- S.D invasion depth into
382 collagen I: MCF-7 57 µm +/- 24, +eGFP 55 µm +/- 22, +LaNt α31-eGFP 50 µm +/- 17,
383 *p*=0.78, determined by ANOVA. Figure S3F. Into Matrigel: MCF-7 55 µm +/- 0, +eGFP 57
384 µm +/- 13, +LaNt α31-eGFP 58 µm +/- 6, *p*>0.71, determined by ANOVA. Figure S3H).

385 **Increased LaNt α31 expression causes a change in mode of invasion**
386 **into laminin-rich hydrogels**

387 In contrast to MCF7, MDA-MB-231 are much more motile and invasive [33, 41, 43].
388 However, the effect of LaNt α31 expression on the 2D migration of MDA-MB-231 was
389 minimal, with a slight, but not statistically significant reduction in gap closure rate (median:
390 MDA-MB-231 98.8 %, +eGFP 92.7 %, +LaNt α31-eGFP 85.1 %, *p*=0.23. Figure 5A-B), and
391 similar outcome in single cell migration assays (mean speed +/- S.D: MDA-MB-231 0.48 µm
392 min^{-1} +/- 0.10, +eGFP 0.50 µm min^{-1} +/- 0.14, +LaNt α31-eGFP 0.36 µm min^{-1} +/- 0.15,
393 MDA-MB-231 vs +LaNt α31-eGFP, *p*=0.16; +eFGP vs +LaNt α31-eGFP, *p*=0.02 determined
394 by ANOVA with Bonferoni post hoc test. Figure 5C-D).
395

Figure 5: LaNt α31 overexpression does not significantly affect 2D migration MDA-MB-231 cells. MDA-MB-231 cells were either left untreated or transduced with eGFP (+eGFP), or LAMA3LN1-eGFP (+LaNt α31-eGFP). For gap closure assays, 24 hours after transduction, cells were seeded into ibidi® 2-well culture inserts and allowed to attach for 6 hours, the inserts were then removed, and the gap margin imaged at 0 hours and 16 hours. For single cell migration assays, 24 hours after transduction, cells were seeded onto tissue culture plastic and the migration paths of individual cells tracked over a four-hour period. (A) Representative images from immediately after removing chamber (T0 upper panels) and after 16 hours (T16 lower panels), yellow lines delineate wound margins. (B) Gap closure was measured as a percentage relative to starting gap area. (C) Vector diagrams showing representative migration paths of 10 individual cells with each colour representing a single cell. (D) Migration speed was measured as total distance migrated over time. Each point on the associated dot plots represents an independent experiment with 2-3 technical replicates per experiment for gap closures assays or 20-40 cells per low density migration assay. Statistical tests of differences relative to controls were performed using one-way ANOVA followed by Bonferroni's post hoc analyses; p>0.05 in all comparisons. Scale bar in (a) represents 100 μm.

As expected MDA-MB-231 invaded into both collagen I and Matrigel matrices (Figure 6). The invasion depth of +LaNt α31-eGFP MDA-MB-231 cells into collagen I was unchanged compared with controls; however, there was a slight reduction in total invasion depth into Matrigel although this did not reach statistical significance compared with both controls once adjusted for multiple comparisons (mean +/- S.D depth into collagen: MDA-MB-231 89 μm +/- 22, +eGFP 90 μm +/- 7, +LaNt α31-eGFP 87 μm +/- 18, p=0.52. Figure 6A-B. Invasion into Matrigel: MDA-MB-231 136 μm +/- 10 S.D, +eGFP 127 μm +/- 4, +LaNt α31-eGFP 97 μm +/- 11, MDA-MB-231 vs +LaNt α31-eGFP p=0.11, +eGFP vs +LaNt α31-eGFP p=0.14, ANOVA with Bonferoni post hoc test. Figure 6C-D).

Figure 6: LaNt α31 overexpression causes a small reduction in invasion of MDA-MB-231 cells into Matrigel. MDA-MB-231 cells, either left untreated or transduced with eGFP (+eGFP), or LAMA3LN1-eGFP (+LaNt α31-eGFP), were plated onto the outside of a transwell membrane. 10 ng mL^{-1} epidermal growth factor was used to stimulate invasion through the membrane into collagen I (A-B) or Matrigel (C-D). After 48 hours, the cells were fixed and DAPI stained then imaged at 5 μm intervals using a spinning disk confocal microscope. (A) and (C) Representative images from 10-40 μm depth presented at equal intervals, with an additional slice at 80 μm in (C). Absolute invasion depth was measured where cell count ≥1. Treatment with GM6001 MMP inhibitor was included as an invasion inhibiting control. Each point on the graphs in (B) and (D) represents an independent experiment, with 2-3 technical replicates per assay. * represents $p<0.05$ between bracketed groups as determined by one-way ANOVA followed by Bonferroni's post hoc analyses.

Although there were minimal differences in invasion depth, visual analysis of the Matrigel invasion assays, revealed an intriguing distinct phenotypic difference between the LaNt α31 overexpressing cells compared with the controls (Figure 6C and 7A). Whereas MDA-MB-231 cells usually invade into Matrigel as multicellular streams, as has been reported previously [43, 44], the +LaNt α31-eGFP cells did not display this behaviour (Movies 1 and 2, maximum intensity projection Figure 7A). To assess this quantitatively, we wrote a macro to convert the DAPI stained images at 60 μm depth into an inverse entropy score as measure of cohesiveness ($entropy^{-1}$) (Figure 7B). At this invasion depth, cell densities were not different between +LaNt α31-eGFP and controls. These analyses agreed with our visual impression that the +LaNt α31-eGFP were less cohesive in their invasion profile (mean +/- S.D $entropy^{-1}$ $x10^{-7}$: MDA-MB-231 1.9 +/- 0.8, +eGFP 2.0 +/- 0.02, +LaNt α31-eGFP 0.93 +/- 0.55, p=0.29. Figure 7C).

Figure 7: LaNt α31 overexpression causes a change in mode of invasion of MDA-MB-231 cells into Matrigel. MDA-MB-231 cells, either left untreated or transduced with eGFP (+eGFP), or LAMA3LN1-eGFP (+LaNt α31-eGFP), were plated onto the outside of a transwell membrane. 10 ng mL^{-1} epidermal growth factor was used to stimulate invasion through the membrane and into Matrigel. After 48 hours, the cells were fixed and stained with DAPI then imaged at 5 μm intervals using a spinning disk confocal microscope. (A) Maximum intensity projection of planes from 20-60 μm from the same assays in Figure 6C. (B) Image analyses method for determining $entropy^{-1}$ as a measure of cell clustering; each stack of images was processed using an automated processing algorithm, where cell count and entropy score after a threshold was measured for each image in the stack. (C) $Entropy^{-1}$ score at 60 μm normalised to pixel intensity plotted to assess clustering of cells.

Tumours with high LaNt α31 expression are likely to be non-cohesive

As the LaNt α31 functional studies data suggested that high expression of this protein changes the mode of tumour invasion, we returned to the tissue array data, focusing specifically on the cores with high LaNt α31 intensity and assessed the tumour appearance in each of those cores as either “cohesive” or “non-cohesive” depending on whether tumour cells were present in contiguous islands with well-defined borders, (representative examples Figure 8A). These analyses revealed that 67.7 % of the high LaNt α31 expressing tumours were non-cohesive in appearance (21 of 31 cores, Figure 8B).

Figure 8: High LaNt α31 expression is associated with low tumour cohesion in invasive ductal carcinoma. Formalin-fixed paraffin embedded human breast tissue microarray sections processed for immunohistochemistry with mouse monoclonal antibodies against LaNt α31. Tumour cohesion was graded as either cohesive (tight tumour islands), or non-cohesive (chord-like) in tumour cores scored as having high LaNt α31 expression. (A)

476 Representative example of core grading. (B) Stacked column graphs of percentage of cases
477 that are either cohesive or non-cohesive. Scale bars: 300 μm.
478

479 Discussion

480 The findings presented here have revealed that the little-known LM-related protein
481 LaNt α31 is upregulated in a distinct sub-population of breast cancers, including a subset of
482 TNBC, but is not definitively predictive of patient outcome. However, the results also show
483 that LaNt α31 is capable of changing the mode of invasion of breast cancer cells into LM-
484 rich matrices, suggesting that dysregulation of this protein could actively contribute to tumour
485 pathology.
486 Usually in tumour situations, very few cells acquire the ability to invade and a
487 hallmark of more aggressive tumours is plasticity in the modes of migration [45, 46]. A switch
488 from multicellular streaming to individual cell invasion can happen in multiple overlapping
489 ways. A major driver is the mechanical properties the ECM including matrix stiffness and the
490 orientation of fibres; however decreased cell-cell adhesion, increased Rac-driven
491 cytoskeletal protrusion compared with Rho-mediated contraction, an increased ability to
492 generate traction forces, and differences in proteolytic activities all can drive the changes
493 [43], as reviewed in [47]. Many of these mechanisms are intrinsically linked, which makes it
494 challenging to directly assign a single behaviour to an individual protein. However, the
495 Matrigel-specific effects and the structural similarity between netrin-4 and LaNt α31 make it
496 tempting to predict that LaNt α31 has a disruptive effect on LM networks, softening and
497 disordering the matrix through which the cells are invading [20, 22]. Matrigel contains many
498 components beyond LM111 [42], therefore the observed phenotype could also be due to
499 LaNt α31 interaction with these additional factors or acting through competition with cell
500 surface receptors. LN domains, including the LN domain of LMα3b, are known to have cell-
501 surface receptor-binding capabilities [48] [49], and notably netrin-4 and a proteolytically
502 released LN domain fragment of LMβ1 are each capable of inducing epithelial to

mesenchymal transition [20, 21, 50, 51]. Dissecting the mechanism of the LaNt α31-induced changes will not be a trivial undertaking but could be valuable to understand the process and as a route toward targeted intervention approaches.

An additional intriguing finding was the difference between LaNt α31 and LMα3. Although these proteins are genetically linked, they are structurally and functionally distinct. Specifically, LMα3a, as part of LM332, has been robustly demonstrated to enhance the migratory behaviour of MCF7 and MDA-MB-231 cells in culture [52, 53]. However, loss or focal disruption of LM332 staining is a more common feature in breast cancer, particularly for LMα3b, which shares a promoter with LaNt α31, and is downregulated in the tumour vasculature [26]. Indeed, in side-by-side comparison of the same tissue, the observation of different structures displaying upregulation of LaNt α31 compared with LMα3 points to differences in post-transcriptional regulation. We do not yet know if the difference is due to differences between the isoforms in terms of pre-mRNA processing, mRNA degradation, or post-translational proteolytic processing; however, these data do suggest that changes to LaNt α31 expression may have more widespread implications to other cancer subtypes where LMα3 is known to be dysregulated. In these contexts, processing tissue for LaNt α31 may have value as a biomarker.

Conclusions

The combination of patient data and manipulative experimental data presented here have revealed LaNt α31, for the first time, to be associated with the progression of breast cancer. Moreover, the finding that LaNt α31 actively influences invasive behaviour indicate that targeting this protein's function could hold potential as a therapeutic approach.

Acknowledgements

This work was supported by Biotechnology and Biological Sciences Research Council Grants BB/L020513/1 and BB/P0257731, and by North West Cancer Research. These funding sources supported the purchase of consumables and equipment access and paid salaries of LDT.

LDT designed and conducted the experiments, analysed the data, and made the figures. TZ assisted in design, analysis and interpretation of the invasion assays. KJH designed the study, analysed data. All authors contributed to the writing and editing of the manuscript. The authors would also like to thank Bryan Williams for his help in writing image analysis macro, Abigail Pickett, Marian Jones, Eleanor Hughes, and Louisa Orfanou for their help in image scoring, and Louise Brown (funded by Breast Cancer Now grant 2014MayPR292) for help with the invasion assays. The authors would like to acknowledge the donors, for without whom, this work would not be possible.

References

1. Hanahan D, Weinberg RA. The hallmarks of cancer. Cell. 2000;100(1):57-70.
2. Sidhom G, Imam M. Evaluation of serum laminin as a tumor marker in breast cancer. Int J Clin Lab Res. 1999;29(1):26-9.
3. Giussani M, Landoni E, Merlino G, Turdo F, Veneroni S, Paolini B, et al. Extracellular matrix proteins as diagnostic markers of breast carcinoma. J Cell Physiol. 2018;233(8):6280-90.
4. Moriggi M, Giussani M, Torretta E, Capitanio D, Sandri M, Leone R, et al. ECM Remodeling in Breast Cancer with Different Grade: Contribution of 2D-DIGE Proteomics. Proteomics. 2018;18(24):e1800278.
5. Holler E. Laminin isoform expression in breast tumors. Breast Cancer Res. 2005;7(4):166-7.
6. Brassart-Pasco S, Brezillon S, Brassart B, Ramont L, Oudart JB, Monboisse JC. Tumor Microenvironment: Extracellular Matrix Alterations Influence Tumor Progression. Front Oncol. 2020;10:397.
7. Hohenester E, Yurchenco PD. Laminins in basement membrane assembly. Cell adhesion & migration. 2013;7(1):56-63.
8. Hamill KJ, Kligys K, Hopkinson SB, Jones JC. Laminin deposition in the extracellular matrix: a complex picture emerges. J Cell Sci. 2009;122(Pt 24):4409-17.
9. Patarroyo M, Tryggvason K, Virtanen I. Laminin isoforms in tumor invasion, angiogenesis and metastasis. Semin Cancer Biol. 2002;12(3):197-207.
10. Rousselle P, Scoazec JY. Laminin 332 in cancer: When the extracellular matrix turns signals from cell anchorage to cell movement. Semin Cancer Biol. 2019.

564 11. Hamill KJ, Langbein L, Jones JC, McLean WH. Identification of a novel family of
565 laminin N-terminal alternate splice isoforms: structural and functional characterization. J Biol
566 Chem. 2009;284(51):35588-96.
567 12. Barrera V, Troughton LD, Iorio V, Liu S, Oyewole O, Sheridan CM, et al. Differential
568 Distribution of Laminin N-Terminus alpha31 Across the Ocular Surface: Implications for
569 Corneal Wound Repair. Invest Ophthalmol Vis Sci. 2018;59(10):4082-93.
570 13. Aumailley M, Bruckner-Tuderman L, Carter WG, Deutzmann R, Edgar D, Ekblom P,
571 et al. A simplified laminin nomenclature. Matrix Biol. 2005;24(5):326-32.
572 14. Ryan MC, Tizard R, VanDevanter DR, Carter WG. Cloning of the LamA3 gene
573 encoding the alpha 3 chain of the adhesive ligand epiligrin. Expression in wound repair. J
574 Biol Chem. 1994;269(36):22779-87.
575 15. Miner JH, Patton BL, Lentz SI, Gilbert DJ, Snider WD, Jenkins NA, et al. The laminin
576 alpha chains: expression, developmental transitions, and chromosomal locations of alpha1-
577 5, identification of heterotrimeric laminins 8-11, and cloning of a novel alpha3 isoform. J Cell
578 Biol. 1997;137(3):685-701.
579 16. Troughton LD, Reuten R, Sugden C, J, Hamill K. Laminin N-terminus α31 protein
580 distribution in adult human tissues. bioRxiv. 2020.
581 17. Iorio V, Troughton LD, Barrera V, Hamill K. LaNt α31 modulates LM332 organisation
582 during matrix deposition leading to cell-matrix adhesion and migration defects. bioRxiv.
583 2019.
584 18. Cheng YS, Champliaud MF, Burgeson RE, Marinkovich MP, Yurchenco PD. Self-
585 assembly of laminin isoforms. J Biol Chem. 1997;272(50):31525-32.
586 19. Yurchenco PD, Cheng YS. Laminin self-assembly: a three-arm interaction hypothesis
587 for the formation of a network in basement membranes. Contrib Nephrol. 1994;107:47-56.
588 20. Schneiders FI, Maertens B, Bose K, Li Y, Brunken WJ, Paulsson M, et al. Binding of
589 netrin-4 to laminin short arms regulates basement membrane assembly. J Biol Chem.
590 2007;282(33):23750-8.
591 21. Staquicini FI, Dias-Neto E, Li J, Snyder EY, Sidman RL, Pasqualini R, et al.
592 Discovery of a functional protein complex of netrin-4, laminin gamma1 chain, and integrin
593 alpha6beta1 in mouse neural stem cells. Proc Natl Acad Sci U S A. 2009;106(8):2903-8.
594 22. Reuten R, Patel TR, McDougall M, Rama N, Nikodemus D, Gibert B, et al. Structural
595 decoding of netrin-4 reveals a regulatory function towards mature basement membranes.
596 Nat Commun. 2016;7:13515.
597 23. Bergstraesser LM, Srinivasan G, Jones JC, Stahl S, Weitzman SA. Expression of
598 hemidesmosomes and component proteins is lost by invasive breast cancer cells. Am J
599 Pathol. 1995;147(6):1823-39.
600 24. Martin KJ, Kwan CP, Nagasaki K, Zhang X, O'Hare MJ, Kaelin CM, et al. Down-
601 regulation of laminin-5 in breast carcinoma cells. Mol Med. 1998;4(9):602-13.
602 25. Henning K, Berndt A, Katenkamp D, Kosmehl H. Loss of laminin-5 in the epithelium-
603 stroma interface: an immunohistochemical marker of malignancy in epithelial lesions of the
604 breast. Histopathology. 1999;34(4):305-9.
605 26. Mori T, Kariya Y, Komiya E, Higashi S, Miyagi Y, Sekiguchi K, et al. Downregulation
606 of a newly identified laminin, laminin-3B11, in vascular basement membranes of invasive
607 human breast cancers. Cancer Sci. 2011;102(5):1095-100.
608 27. Carpenter PM, Wang-Rodriguez J, Chan OT, Wilczynski SP. Laminin 5 expression in
609 metaplastic breast carcinomas. Am J Surg Pathol. 2008;32(3):345-53.
610 28. Soule HD, Vazguez J, Long A, Albert S, Brennan M. A human cell line from a pleural
611 effusion derived from a breast carcinoma. J Natl Cancer Inst. 1973;51(5):1409-16.
612 29. Cailleau R, Young R, Olive M, Reeves WJ, Jr. Breast tumor cell lines from pleural
613 effusions. J Natl Cancer Inst. 1974;53(3):661-74.
614 30. O'Brien J, Wilson I, Orton T, Pognan F. Investigation of the Alamar Blue (resazurin)
615 fluorescent dye for the assessment of mammalian cell cytotoxicity. Eur J Biochem.
616 2000;267(17):5421-6.

617 31. Oppelt A, Haugsten EM, Zech T, Danielsen HE, Sveen A, Lobert VH, et al. PIKfyve,
618 MTMR3 and their product PtdIns5P regulate cancer cell migration and invasion through
619 activation of Rac1. Biochem J. 2014;461(3):383-90.
620 32. Garcia E, Ragazzini C, Yu X, Cuesta-Garcia E, Bernardino de la Serna J, Zech T, et
621 al. WIP and WICH/WIRE co-ordinately control invadopodium formation and maturation in
622 human breast cancer cell invasion. Sci Rep. 2016;6:23590.
623 33. MacDonald E, Brown L, Selvais A, Liu H, Waring T, Newman D, et al. HRS-WASH
624 axis governs actin-mediated endosomal recycling and cell invasion. J Cell Biol.
625 2018;217(7):2549-64.
626 34. Kleinman HK, Martin GR. Matrigel: basement membrane matrix with biological
627 activity. Semin Cancer Biol. 2005;15(5):378-86.
628 35. Lu Z, Jiang G, Blume-Jensen P, Hunter T. Epidermal growth factor-induced tumor
629 cell invasion and metastasis initiated by dephosphorylation and downregulation of focal
630 adhesion kinase. Mol Cell Biol. 2001;21(12):4016-31.
631 36. Gerdes J, Lemke H, Baisch H, Wacker HH, Schwab U, Stein H. Cell cycle analysis of
632 a cell proliferation-associated human nuclear antigen defined by the monoclonal antibody Ki-
633 67. J Immunol. 1984;133(4):1710-5.
634 37. Dowsett M, Nielsen TO, A'Hern R, Bartlett J, Coombes RC, Cuzick J, et al.
635 Assessment of Ki67 in breast cancer: recommendations from the International Ki67 in Breast
636 Cancer working group. J Natl Cancer Inst. 2011;103(22):1656-64.
637 38. Kligys K, Wu Y, Hamill KJ, Lewandowski KT, Hopkinson SB, Budinger GR, et al.
638 Laminin-332 and alpha3beta1 integrin-supported migration of bronchial epithelial cells is
639 modulated by fibronectin. Am J Respir Cell Mol Biol. 2013;49(5):731-40.
640 39. Hamill KJ, Hopkinson SB, Hoover P, Todorovic V, Green KJ, Jones JC. Fibronectin
641 expression determines skin cell motile behavior. J Invest Dermatol. 2012;132(2):448-57.
642 40. Hamill KJ, Hiroyasu S, Colburn ZT, Ventrella RV, Hopkinson SB, Skalli O, et al.
643 Alpha actinin-1 regulates cell-matrix adhesion organization in keratinocytes: consequences
644 for skin cell motility. J Invest Dermatol. 2015;135(4):1043-52.
645 41. Yu X, Zech T, McDonald L, Gonzalez EG, Li A, Macpherson I, et al. N-WASP
646 coordinates the delivery and F-actin-mediated capture of MT1-MMP at invasive pseudopods.
647 J Cell Biol. 2012;199(3):527-44.
648 42. Hughes CS, Postovit LM, Lajoie GA. Matrigel: a complex protein mixture required for
649 optimal growth of cell culture. Proteomics. 2010;10(9):1886-90.
650 43. Wolf K, Wu YI, Liu Y, Geiger J, Tam E, Overall C, et al. Multi-step pericellular
651 proteolysis controls the transition from individual to collective cancer cell invasion. Nat Cell
652 Biol. 2007;9(8):893-904.
653 44. Scott RW, Hooper S, Crighton D, Li A, Konig I, Munro J, et al. LIM kinases are
654 required for invasive path generation by tumor and tumor-associated stromal cells. J Cell
655 Biol. 2010;191(1):169-85.
656 45. Pinner S, Sahai E. Imaging amoeboid cancer cell motility in vivo. J Microsc.
657 2008;231(3):441-5.
658 46. Farina KL, Wyckoff JB, Rivera J, Lee H, Segall JE, Condeelis JS, et al. Cell motility
659 of tumor cells visualized in living intact primary tumors using green fluorescent protein.
660 Cancer Res. 1998;58(12):2528-32.
661 47. Friedl P, Wolf K. Plasticity of cell migration: a multiscale tuning model. J Cell Biol.
662 2010;188(1):11-9.
663 48. Garbe JH, Gohring W, Mann K, Timpl R, Sasaki T. Complete sequence, recombinant
664 analysis and binding to laminins and sulphated ligands of the N-terminal domains of laminin
665 alpha3B and alpha5 chains. Biochem J. 2002;362(Pt 1):213-21.
666 49. Kariya Y, Yasuda C, Nakashima Y, Ishida K, Tsubota Y, Miyazaki K. Characterization
667 of laminin 5B and NH2-terminal proteolytic fragment of its alpha3B chain: promotion of
668 cellular adhesion, migration, and proliferation. J Biol Chem. 2004;279(23):24774-84.
669 50. Horejs CM, Serio A, Purvis A, Gormley AJ, Bertazzo S, Poliniewicz A, et al.
670 Biologically-active laminin-111 fragment that modulates the epithelial-to-mesenchymal
671 transition in embryonic stem cells. Proc Natl Acad Sci U S A. 2014;111(16):5908-13.

672 51. Xu X, Yan Q, Wang Y, Dong X. NTN4 is associated with breast cancer metastasis
673 via regulation of EMT-related biomarkers. Oncol Rep. 2017;37(1):449-57.
674 52. Plopper GE, Domanico SZ, Cirulli V, Kiosses WB, Quaranta V. Migration of breast
675 epithelial cells on Laminin-5: differential role of integrins in normal and transformed cell
676 types. Breast Cancer Res Treat. 1998;51(1):57-69.
677 53. Carpenter PM, Sivadas P, Hua SS, Xiao C, Gutierrez AB, Ngo T, et al. Migration of
678 breast cancer cell lines in response to pulmonary laminin 332. Cancer Med. 2017;6(1):220-
679 34.
680

681 # Supporting information

682 **Figure S1: LaNt α31 is upregulated in ductal carcinoma and in lymph node**
683 **metastases.** Formalin-fixed paraffin-embedded human breast tissue microarray sections
684 processed for immunohistochemistry with mouse monoclonal antibodies against LaNt α31.
685 Two separate arrays were used; (A) uninvolved with paired invasive/ in situ ductal carcinoma
686 tissues (N=25), (B) invasive ductal carcinoma with paired node metastases (N=29). All
687 paired cores analysed in Figure 2 ordered based on LaNt α31 staining intensity, low to high
688 (left to right). Scale bars: 500 μm.
689

690 **Figure S2: LaNt α31 overexpression does not affect cell metabolism.** MCF-7 or MDA-
691 MB-231 cells, either left untreated or transduced with eGFP (+eGFP), or LAMA3LN1-eGFP
692 (+LaNt α31-eGFP), were maintained for 48 hours following transduction. (A) Immunoblots
693 from total cell lysates for MCF-7 or MDA-MB-231 cells probed with antibodies against LaNt
694 α31, with ponceau S total protein stained membrane below. (B) Resazurin salts (44 μM)
695 were added to transduced cells for 2 hours, then the fluorescence intensity of the culture
696 medium was measured at 570 nm. Dot plot of fluorescence intensity relative to non-
697 transduced cells.
698

699 **Figure S3: LaNt α31 overexpression does not significantly affect 2D migration or 3D**
700 **invasion of MCF-7 cells.** MCF-7 cells were either left untreated or transduced with eGFP
701 (+eGFP), or LAMA3LN1-eGFP (+LaNt α31-eGFP). For gap closure assays, 24 hours after
702 transduction, cells were seeded into ibidi® 2-well culture inserts and allowed to attach for 6

703 hours, the inserts were then removed, and the gap margin imaged at 0 hours and 16 hours.
704 For single cell migration assays, 24 hours after transduction, cells were seeded onto tissue
705 culture plastic and the migration paths of individual cells tracked over a four-hour period. (A)
706 Representative images from immediately after removing chamber (T0 upper panels) and
707 after 16 hours (T16 lower panels), yellow lines delineate wound margins. (B) Gap closure
708 was measured as a percentage relative to starting gap area. (C) Vector diagrams showing
709 representative migration paths of 10 individual cells with each colour representing a single
710 cell. (D) Migration speed was measured as total distance migrated over time. Each point on
711 the associated dot plots represents an independent experiment with 2-3 technical replicates
712 per experiment for gap closures assays or 20-40 cells per low density migration assay. For
713 invasion assays, cells were plated onto the outside of a transwell membrane. 10 ng mL^{-1}
714 epidermal growth factor was used to stimulate invasion through the membrane and into
715 collagen I or Matrigel. After 48 hours, the cells were fixed and stained with DAPI then
716 imaged at 5 μm intervals using a spinning disk confocal microscope. (E and G)
717 Representative images of invasion into collagen I or Matrigel from 10-40 μm presented at
718 equal intervals. (F and H) Absolute invasion depth was measured where cell count ≥1.
719 Treatment with GM6001 MMP inhibitor was included as an invasion inhibiting control. Each
720 point on the graphs represents an independent experiment, with 2-3 technical replicates per
721 assay. * represents $p<0.05$ between bracketed groups as determined by one-way ANOVA
722 followed by Bonferroni's post hoc analyses. Statistical tests of differences relative to controls
723 were performed using one-way ANOVA followed by Bonferroni's post hoc analyses; $p>0.05$
724 in all comparisons. Scale bar in (a) represents 100 μm.
725

726 **Movie 1: MDA-MB-231 +eGFP invasion into Matrigel (.avi)**

727 MDA-MB-231 cells transduced with eGFP were plated onto the outside of a transwell
728 membrane. 10 ng mL^{-1} epidermal growth factor was used to stimulate invasion through the
729 membrane and into Matrigel. After 48 hours, the cells were fixed and stained with DAPI then

730 imaged at 5 μm intervals using a spinning disk confocal microscope. Representative movie
731 of invasion profile generated from z-stack slices for invasion between 20 and 60 μm after
732 applying threshold.
733

734 **Movie 2: MDA-MB-231 +LaNt α31-eGFP invasion into Matrigel (.avi).** MDA-MB-231 cells
735 transduced with LaNt α31-eGFP were plated onto the outside of a transwell membrane. 10
736 ng mL^{-1} epidermal growth factor was used to stimulate invasion through the membrane and
737 into Matrigel. After 48 hours, the cells were fixed and stained with DAPI then imaged at 5 μm
738 intervals using a spinning disk confocal microscope. Representative movie of invasion profile
739 generated from z-stack slices for invasion between 20 and 60 μm after applying threshold.
740

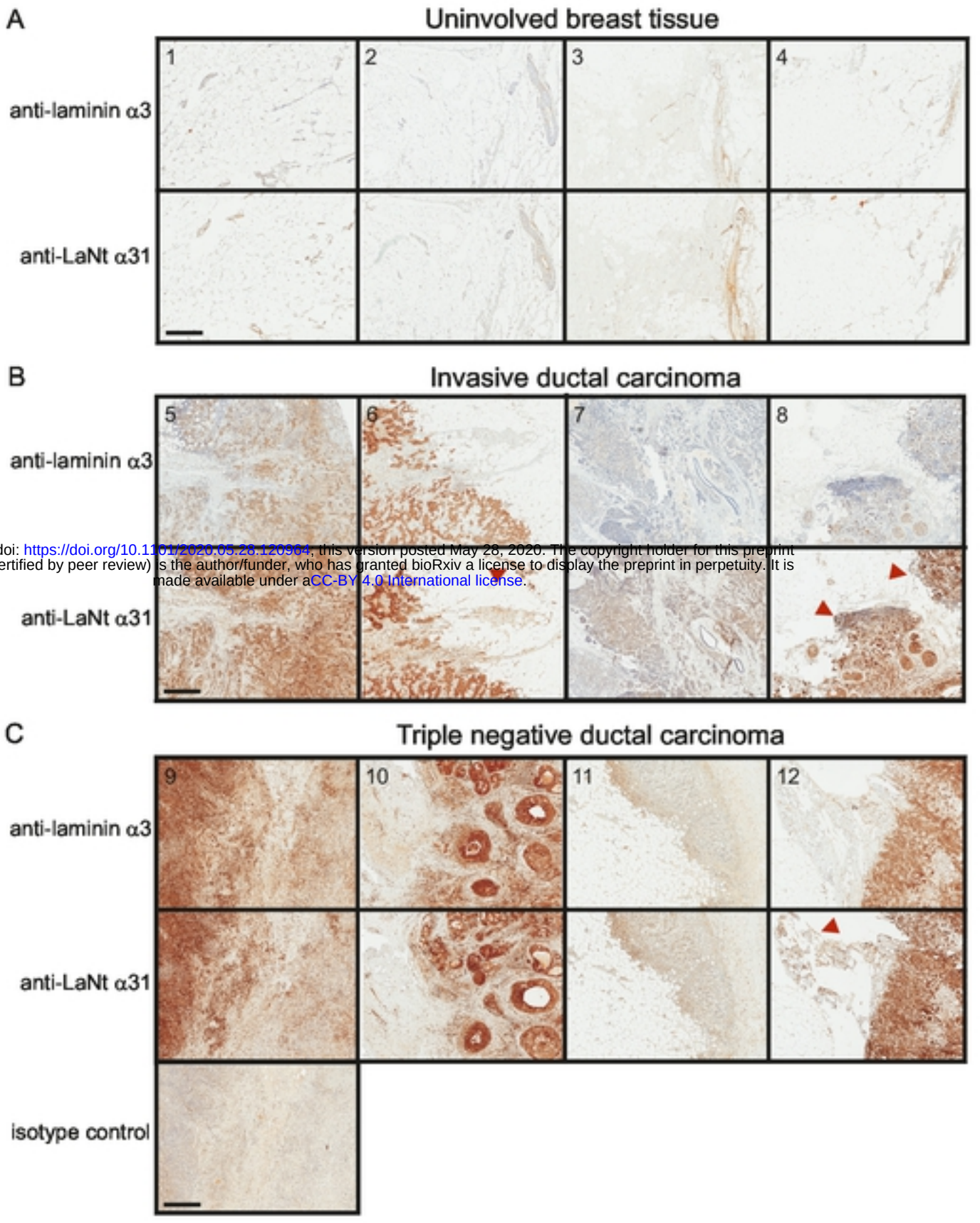

Figure 1

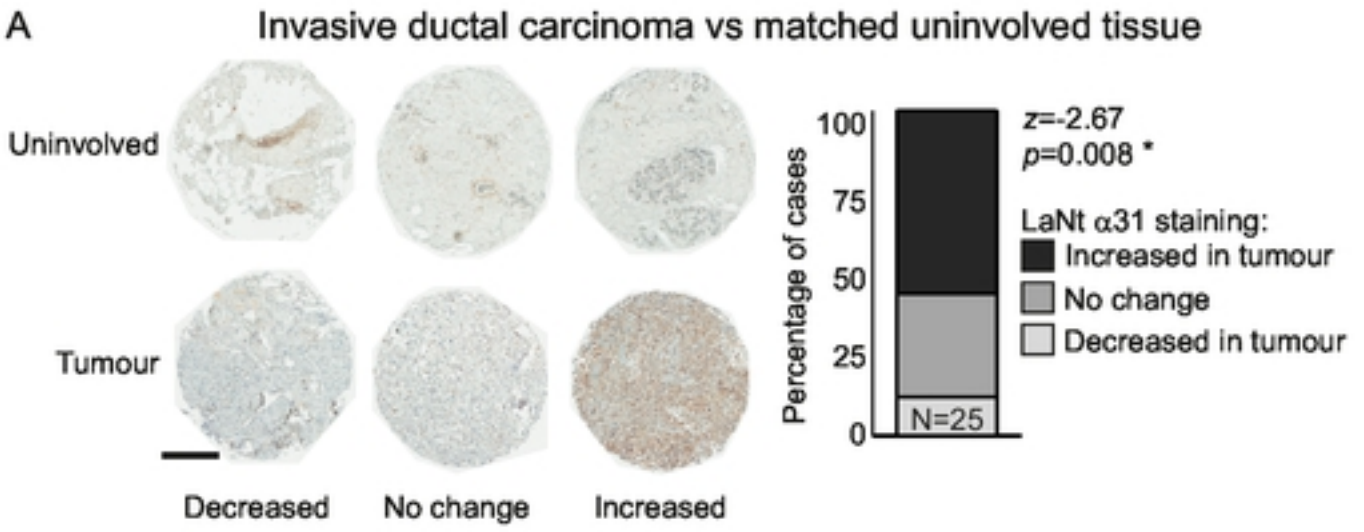

Figure 2

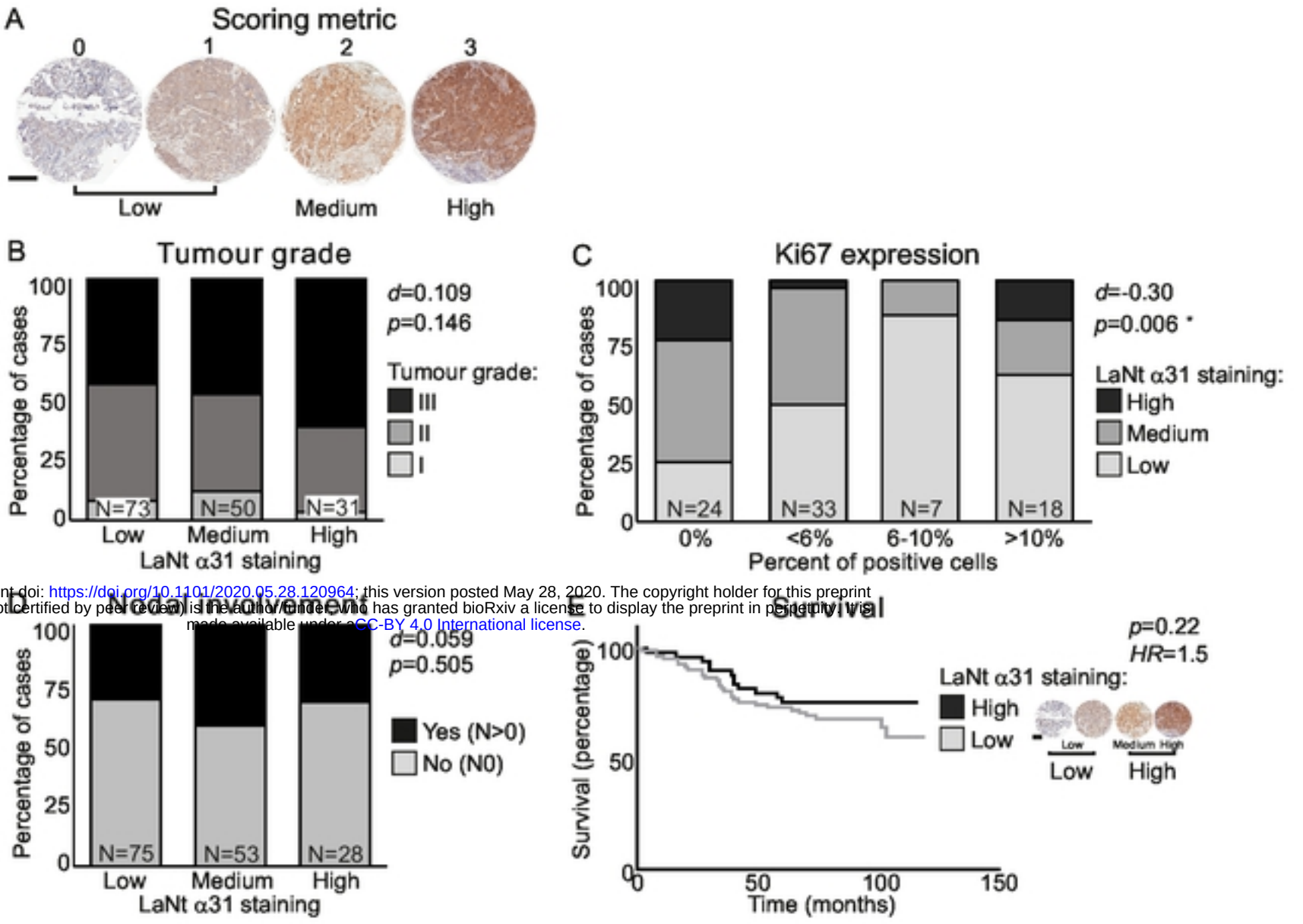

Figure 3

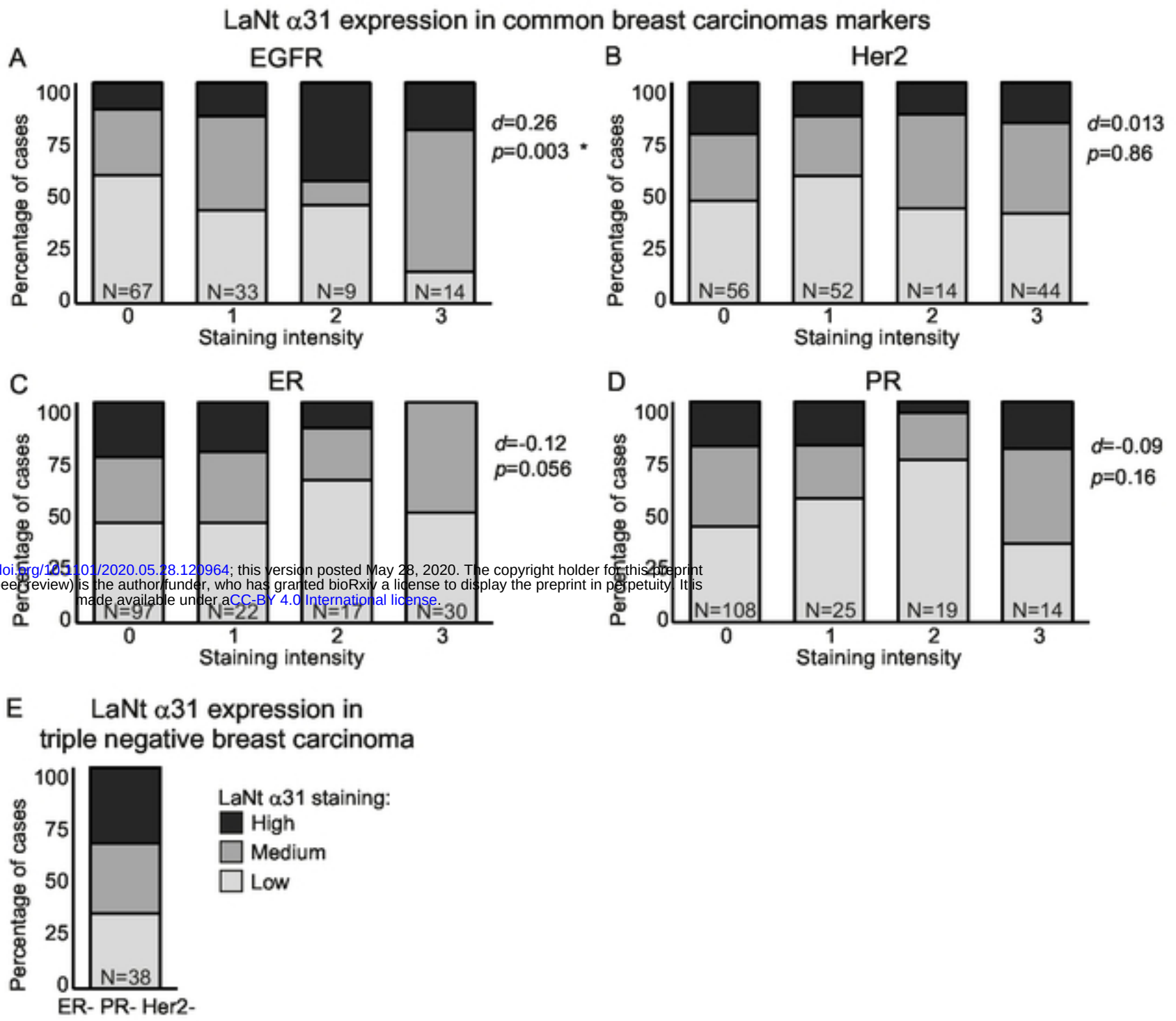

Figure 4

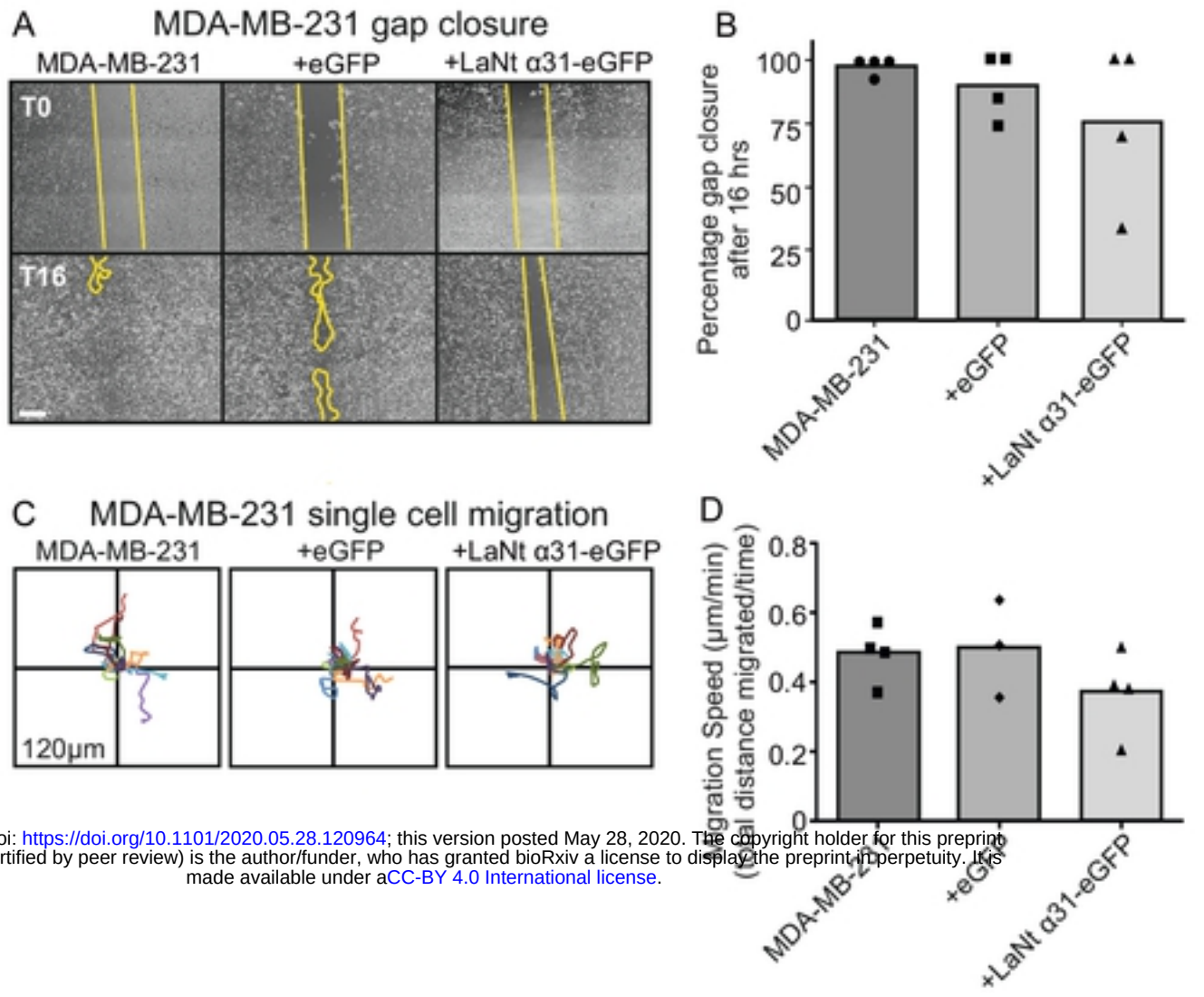

Figure 5

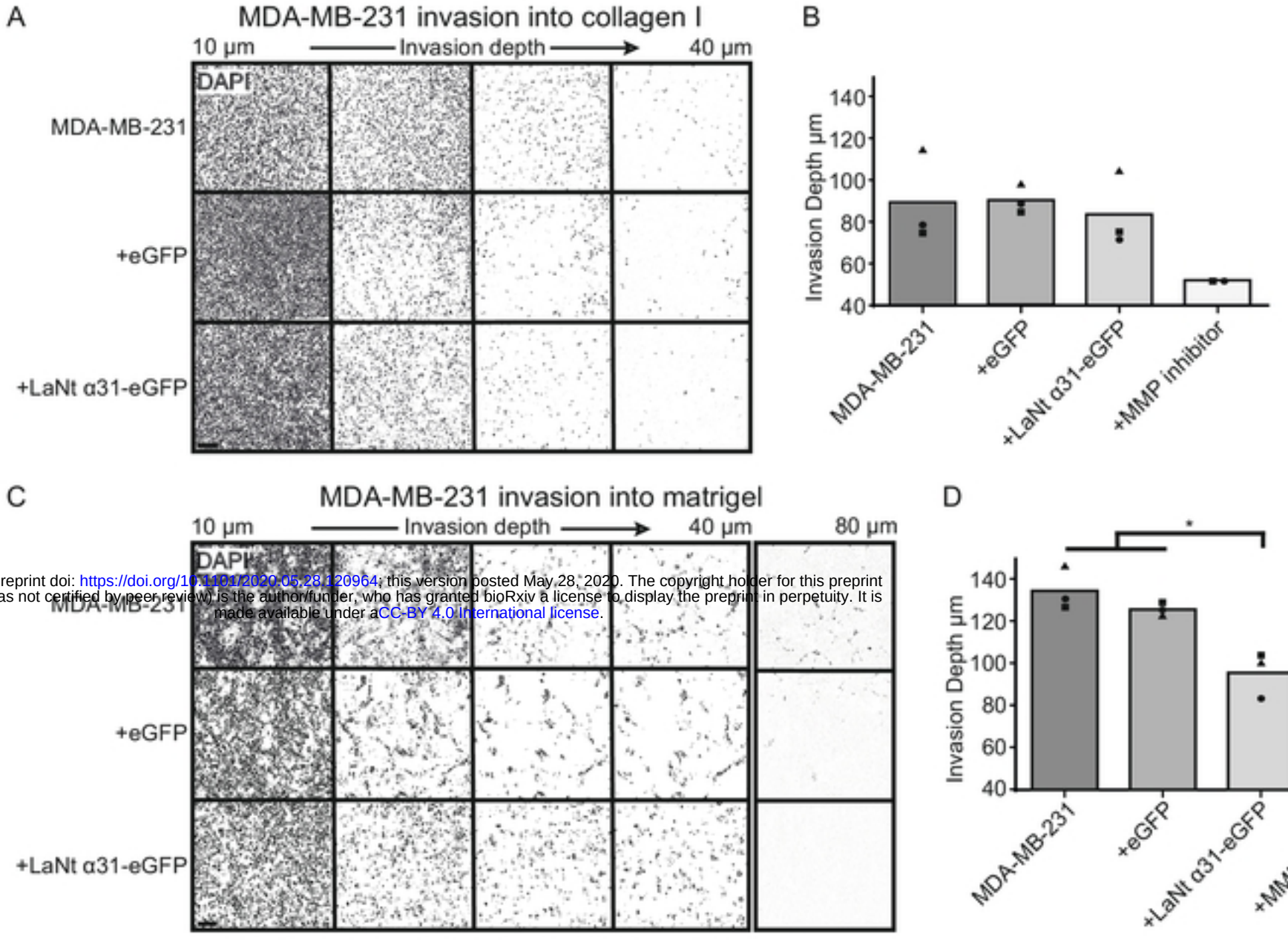

Figure 6

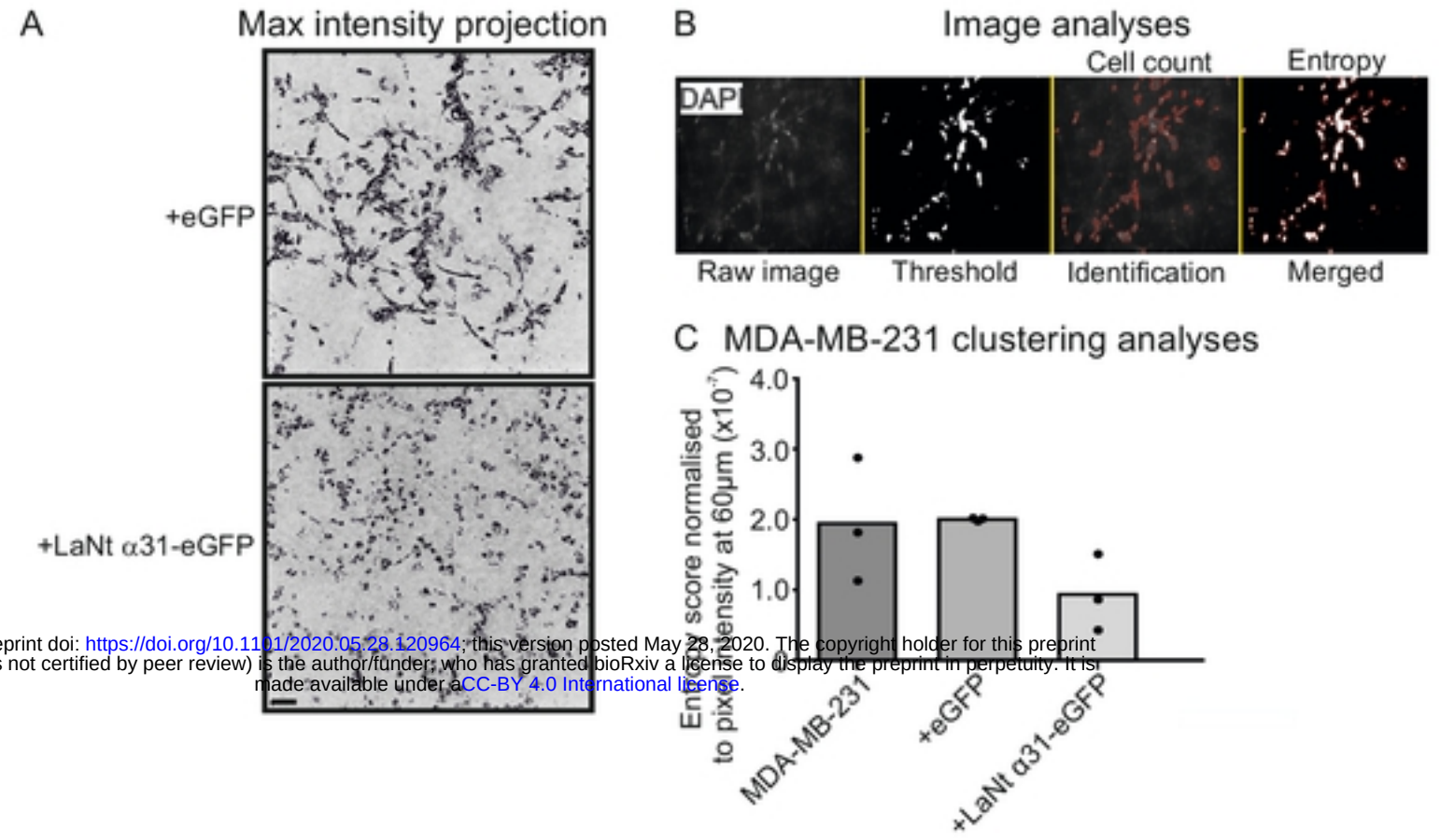

Figure 7

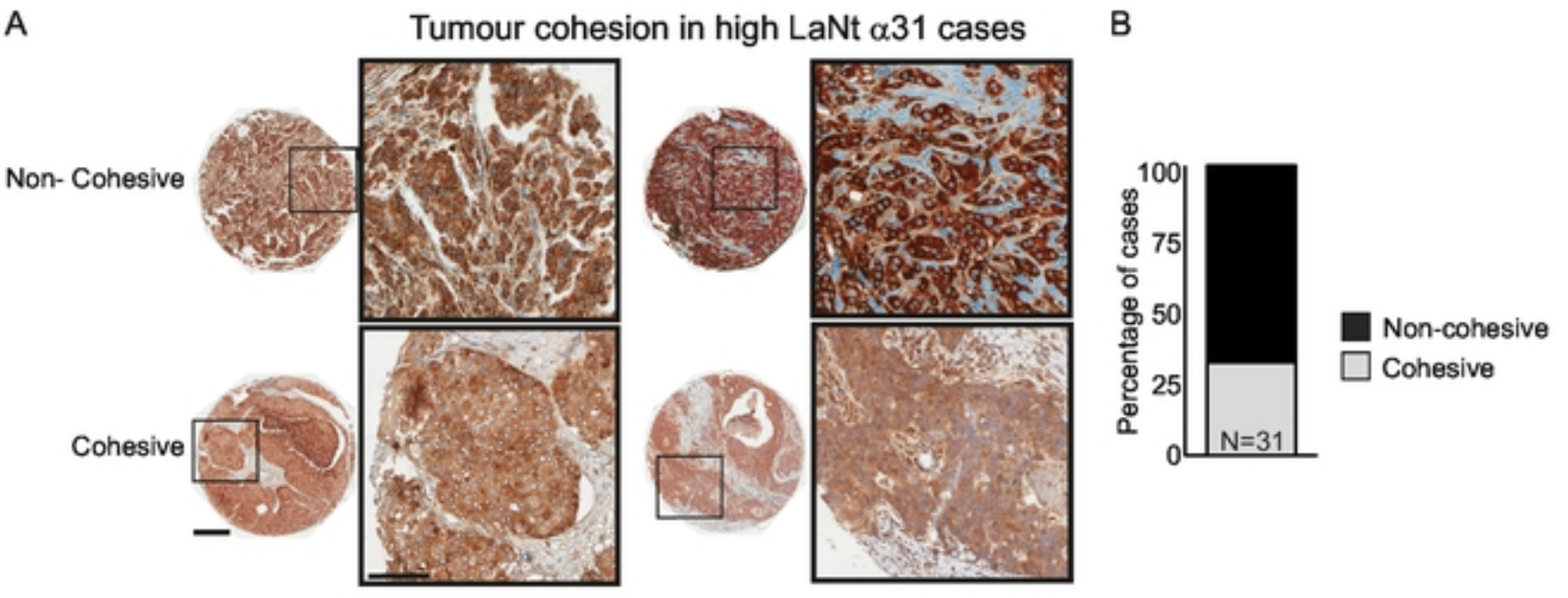

Figure 8